Proceedings of the ASME 2024 19th International Manufacturing Science and Engineering Conference
MSEC2024
June 17-21, 2024, Knoxville, Tennessee

MSEC2024-123863

IN-PROCESS MONTIROING OF PROCESS STABILITY IN LASER WIRE DIRECTED ENERGY DEPOSITION USING PHYSICS-BASED MACHINE LEARNING

Ben Bevans
Virginia Tech
Blacksburg, VA

Anis Assad
PUCPR
Curitiba, Brazil

Jakob Hamilton
Iowa State
Ames, Iowa

Prahalada Rao
Virginia Tech
Blacksburg, VA

Iris Rivero
University of Florida
Gainesville, FL

ABSTRACT

The objective of this work is to detect process instabilities in laser wire directed energy deposition additive manufacturing process using real-time data from a high-speed imaging meltpool sensor. The laser wire directed energy deposition process combines the advantages of powder directed energy deposition and other wire-based additive manufacturing processes, such as wire arc additive manufacturing, as it provides both appreciable resolution and high deposition rates. However, the process tends to create sub-optimal quality parts with poor surface finish, geometric distortion, and delamination in extreme cases. This sub-optimal quality stems from poorly understood thermophysical phenomena and stochastic effects. Hence, flaw formation often occurs despite considerable effort to optimize the processing parameters. In order to overcome this limitation of laser wire directed energy deposition, real-time and accurate monitoring of the process quality state is the essential first step for future closed-loop quality control of the process. In this work we extracted low-level, physically intuitive, features from acquired meltpool images. Physically intuitive features such as meltpool shape, size, and brightness provide a fundamental understanding of the processing regimes that are understandable by human operators. These physically intuitive features were used as inputs to simple machine learning models, such as k-nearest neighbors, support vector machine, etc., trained to classify the process state into one of four possible regimes. Using simple machine learning models forgoes the need to use complex black box modeling such as convolutional neural networks to monitor the high speed meltpool images to determine process stability. The classified regimes identified in this work were stable, dripping, stubbing, and incomplete melting. Regimes such as dripping, stubbing, and incomplete melting regimes fall under the realm of unstable processing conditions that are liable to lead to flaw formation in the laser wire directed energy deposition process. The foregoing three process regimes are the primary source of sub-optimal quality parts due to the degradation of the single-track quality that are the fundamental building block of all manufactured samples. Through a series of single-track experiments conducted over 128 processing conditions, we show that the developed approach is capable of accurately classifying the process state with a statistical fidelity approaching 90% F-score. This level of statistical fidelity was achieved using eight physically intuitive meltpool morphology and intensity features extracted from 159,872 meltpool images across all 128 process conditions. These eight physically intuitive features were then used for the training and testing of a support vector machine learning model. This prediction fidelity achieved using physically intuitive features is at par with computationally intense deep learning methods such as convolutional neural networks.

Keywords: Additive Manufacturing, Laser Wire Directed Energy Deposition, Machine Learning, High-Speed Imaging, In-situ Monitoring

1. INTRODUCTION

1.1 Goal and Motivation

This work aims to mitigate flaw formation in the laser wire directed energy deposition (LW-DED) additive manufacturing process, shown in FIGURE 1(a). In LW-DED, material in the form of wire is melted using energy from a laser and deposited layer-upon-layer. The relative movement of the wire and laser by a moving stage enables the creation of complex, large volume, near net shape parts.

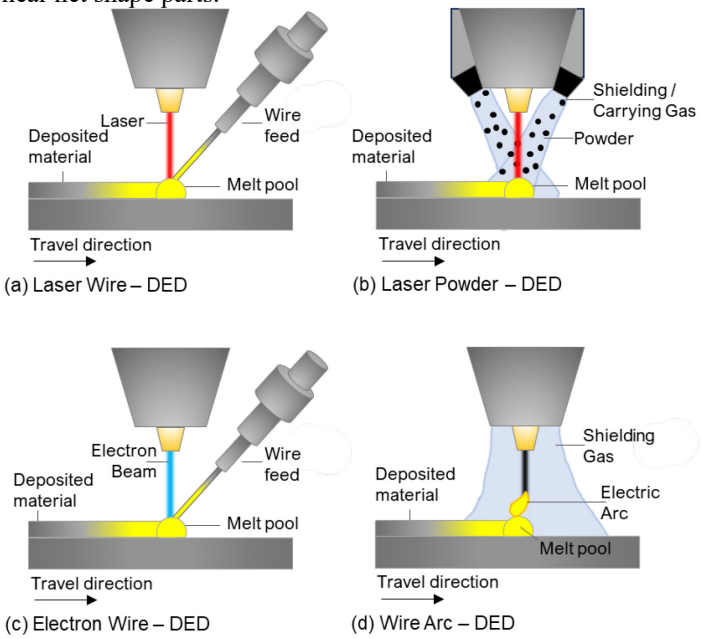

FIGURE 1: DEPICTION OF; (A) LASER WIRE DIRECTED ENERGY DEPOSITION (DED) PROCESS, (B) LASER POWDER DED, (C) ELCTRON WIRE DED, AND (D) WIRE ARC DED.

The LW-DED process is closely related to the wire arc directed energy deposition (WA-DED), and laser powder directed energy deposition (LP-DED). In the former, the wire is melted using energy from an electric arc, and in the latter, the material is sprayed from a nozzle in powder form. While WA-DED deposits large volumes of material, it has poor geometric integrity and surface finish. This leads to a substantial amount of post-process machining. Aspects of the LP-DED, LW-DED, and WA-DED, and electron beam DED (EB-DED) are juxtaposed in TABLE 1. By contrast, LP-DED has higher geometric integrity and surface finishes but has a substantially lower volumetric deposition rate compared to that of the other DED processes.

In this context, LW-DED combines the precision of LP-DED with the large volume deposition capability of WA-DED. Consequently, the process is of growing interest in the aerospace industry of manufacturing large components, such as rocket nose cones in a rapid and cost-effective manner to near net-shape.

However, production-level scale of the LW-DED process is currently hindered due to the tendency of the process instability, despite extensive process optimization. This process instability results in malformed parts with flaws and poor geometric integrity. Select process drifts resulting in sub-optimal deposit geometries are summarized in FIGURE 4. Such process drifts are caused by poorly understood laser-material interactions, complex thermal physics, and sensitivity to stochastic disturbances. Accordingly, to ensure industrial viability of LW-DED it is necessary to continually monitor the process using data from in-process sensors so that process drifts can be detected and corrected before they cascade to succeeding layers.

TABLE 1: COMPARISON OF THE VARIOUS TYPES OF DED.

	LP-DED	LW-DED	EW-DED	WA-DED
Feedstock Material	Powder	Wire	Wire	Electrode
Energy Source	Laser	Laser	Electron Beam	Plasma Arc
Deposition Rate [kg·hr^{-1}]	2.2	3.0	9.0	10.0
Resolution	0.2 mm	0.5 mm	0.5 mm	1.0 mm

1.2 Objective and Approach

The objective of this work is to monitor the LW-DED process in-situ with a meltpool (weldpool) imaging sensor to detect process instabilities. The underlying hypothesis is that the laser-material interactions, symptomatic of process drifts, manifest in the meltpool behavior, specifically, the shape and intensity of the meltpool. Consequently, tracking of meltpool dynamics with simple machine learning models would enable accurate detection of an incipient process drift.

In this work, we use data from an in-process high-speed camera to acquire images of the meltpool and its surrounding region. Subsequently, images of the meltpool are analyzed using machine vision algorithms. These machine vision algorithms provide quantitative features (process signatures) pertaining to the meltpool dynamics, such as shape, intensity, eccentricity, etc., are extracted. These process signatures are used as inputs to a simple machine learning model trained to classify the process state into one of four possible regimes: stable, dripping, stubbing, and incomplete melting.

If the LW-DED process stays in one of the three unstable processing conditions, various types of malformed parts will form. Continuous deposition of the dripping regime will form parts with poor surface finish that will affect the deposition of future layers. Stubbing, if not corrected, will generate parts with both poor surface finish and with the excessive feedstock wire sticking out of the part. Finally, if incomplete melting continues it will result in no part being formed. Hence, these processing conditions are important to monitor and predict prior to catastrophic part failure.

1.3 Prior Work & Novelty

In the literature, there is very little work performed on flaw detection and process monitoring in LW-DED. Most current works focus on better understanding the fundamental processes. In work done by Abioye et al. [1], they did a comprehensive parameter study changing scan speed and laser power to develop a process map of stability, dripping, stubbing, and incomplete

melting. Work done by Motta et al. [2], monitored the meltpool with a high-speed camera during a parameter study to visualize the change in the meltpool morphology at different processing regimes. Similarly, To build upon these works, Gibson et al. [3] and Chen et al. [4] use an integrated camera to control and maintain a constant meltpool area or width (respectively) via a closed loop controller to modulate the laser power. These works found that by controlling the meltpool morphology, the geometric integrity of the sample was increased.

One of the few works done on quality prediction in Laser Wire – DED was performed by Jamnikar et al. [5]. In this work, they predicted the resultant track penetration depth, height, width, and height. However, this prediction was done using a complex Convolutional Neural Network (CNN) and a high-speed camera. While powerful, CNNs require the storage of thousands of images that can be computationally expensive if the data needs to be stored.

TABLE 2: LITERATURE REVIEW TABLE FOR LW-DED

Complexity	Ref.	Sensor	Task
Process Understanding	[1]	None	Process mapping
Correlation to Meltpool	[2]	Integrated Camera	Meltpool to Regime Visualization
Control of Meltpool	[3, 4]	Integrated Camera	Maintain constant Meltpool Width
Prediction of Quality	[5]	High-Speed Camera	Use CNN to Predict Track Quality

In this work, we developed a computer vision algorithm that can extract physics-based monitoring features from the meltpool monitoring high-speed camera. From these monitoring features, simple machine learning models were generated to predict the track quality regime of stable, dripping, incomplete melting, and stubbing. This methodology allows for the monitoring features to be saved in a less computationally expensive way and still monitor the track quality.

2. METHODS

2.1 Experimental Setup

A Hybrid Manufacturing Technologies (AMBIT FLEX) wire-feed system was integrated into a Hardinge GX250-5ax milling machine to perform LW-DED. The laser source was a 2kW 1070 nm IPG Photonics Yb-doped fiber laser. The laser generated a 2 mm spot size and was protected with argon shielding gas ejected at 20 L·min^{-1}. Data was collected in-situ with an Edgertronic SC2+ high-speed camera, mounted off-axis at 45º, shown in FIGURE 2. Images were captured at 2,500 Hz with a 1280×720 pixel resolution at a spatial resolution of 20 µm per pixel.

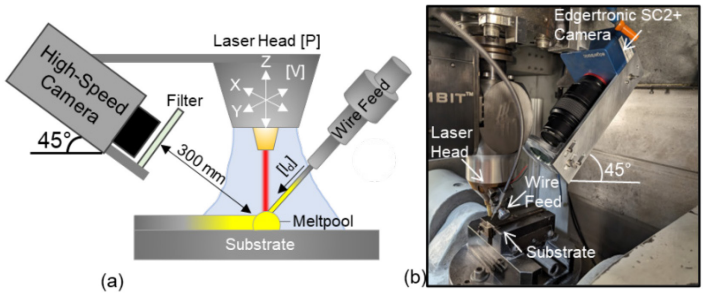

FIGURE 2: (A) APPARATUS SCHEMATIC: INCIDENT WIRE IS MELTED BY THE LASER, AS IN-SITU IMAGE MONITORING IS PERFORMED BY AN OFF-AXIS HIGH-SPEED CAMERA.

2.2 Design of Experiments

Stainless steel 316L wire from Lincoln Electric (1.1 mm diameter) was used as feedstock for 128 printed 40 mm long single-tracks. Each single-track was produced under distinct process parameters in full factor design of experiment, visualized in FIGURE 3, with three main variables: laser power (P, [W]), scanning velocity (V, [mm·s^{-1}]), and linear mass density (l_d, [g·mm^{-1}]). Linear mass density refers to the ratio of the temporal material feeding rate and the laser scanning speed. This ensures similar material deposition per unit length of printing. An inordinately large l_d would lead to large accumulation of material ahead of the meltpool, characteristic of stubbing.

Laser power varied between 600 W to 1800 W and scanning speed varied between 250 mm·min^{-1} to 1500 mm·min^{-1}. This resulted in 64 distinct laser power and scan speed treatments. To add another dimension to the experiment, two linear mass densities were studied, one at 0.0086 g·mm^{-1} and one at 0.0129 g·mm^{-1}, shown in FIGURE 3. Both linear mass densities studied had the same 64 treatment conditions resulting in 128 distinct treatment conditions, one for each single-track studied.

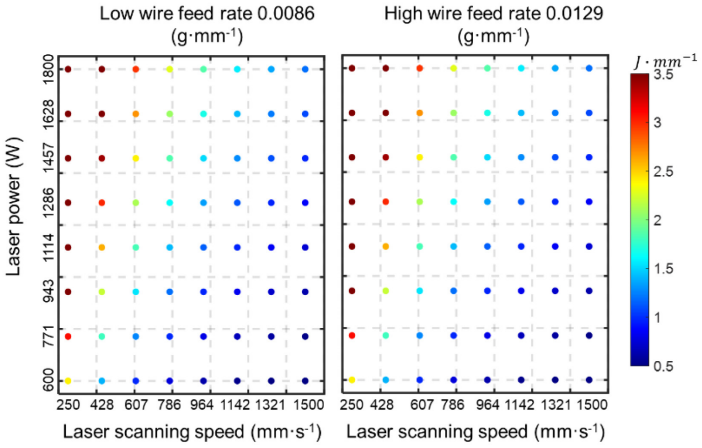

FIGURE 3: 128 DISTINCT PROCESSING PARAMETERS USED IN THE EXPERIMENT.

Depicted in FIGURE 4 are the four process regimes observed in this study. These quality regimes are stable FIGURE 4(a), stubbing FIGURE 4(b), dripping FIGURE 4(c), and

incomplete melting FIGURE 4(d). Stubbing results from insufficient energy to melt both the incident wire and substrate leading to semi-solid wire protruding from the surface of the meltpool. The dripping regime is caused by excess energy delivery to the wire which melts the wire prior to meltpool leading the melted material to 'drip' onto the substrate [2, 6]. Incomplete melting is characterized by either insufficient energy or insufficient material delivery resulting in a deficiently small meltpool that is unable to deposit a single-track.

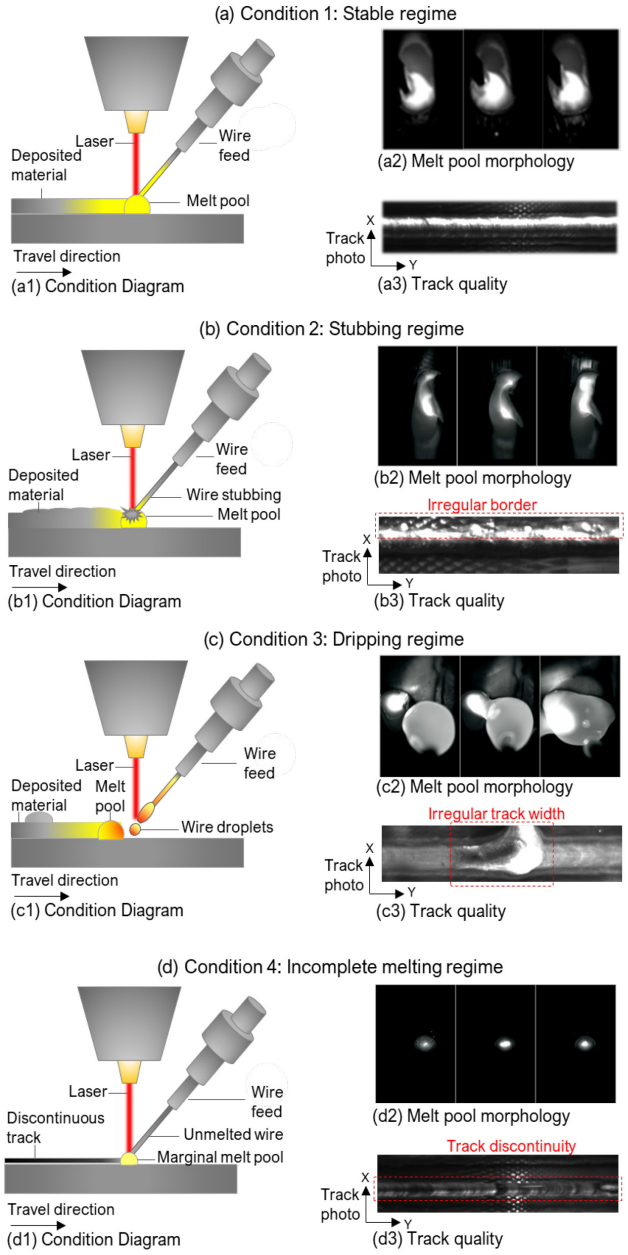

FIGURE 4: DEPICTION OF THE THREE INSTABILITY PROCESSING REGIMES, THEIR MELTPOOL MORPHOLOGIES, AND THEIR EFFECT ON THE QUALITY OF THE TRACK. (B) STUBBING REGIME: (C) DRIPPING REGIME (D) INCOMPLETE MELTING REGIME.

2.3 Machine Learning

Computer vision and machine learning were applied to analyze the captured meltpool images and detect which quality regime is being generated. To perform this work the developed approach first used simple computer vision to identify the meltpool boundary. Second the developed approach extracted physically intuitive features to monitor the process. Third and final, simple machine learning models were developed to perform the classification of quality regime.

Detection of the meltpool contour was performed by first taking the raw high-speed image and applying a gaussian blurring filter to remove noise and highlight key features of the image (FIGURE 5(1-2)). Then binary thresholding was performed on blurred image, (FIGURE 5(3)), to identify the pixels associated with molten material. The final step, (FIGURE 5(4)), implemented a border tracing algorithm to identify the contour of the meltpool generated in the process. All computer vision algorithms were computationally implemented in Python 3.7 with the support of the OpenCV library.

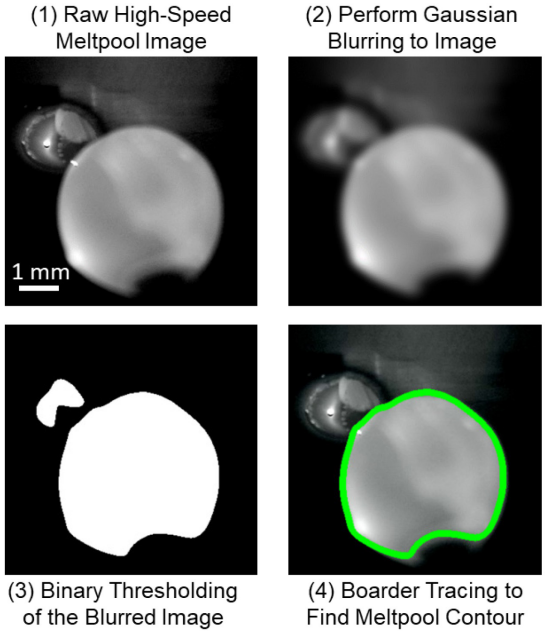

FIGURE 5: DEPICTION OF THE COMPUTER VISION APPROACH OF IDENTIFYING THE CONTOUR OF THE MELTPOOL FROM THE RAW HIGH-SPEED IMAGE.

A supervised classification approach was utilized to predict the four process regimes (*i.e.*, dripping, incomplete melting, stubbing, and stable) based on the selected meltpool morphology and intensity-based features depicted in FIGURE 6.

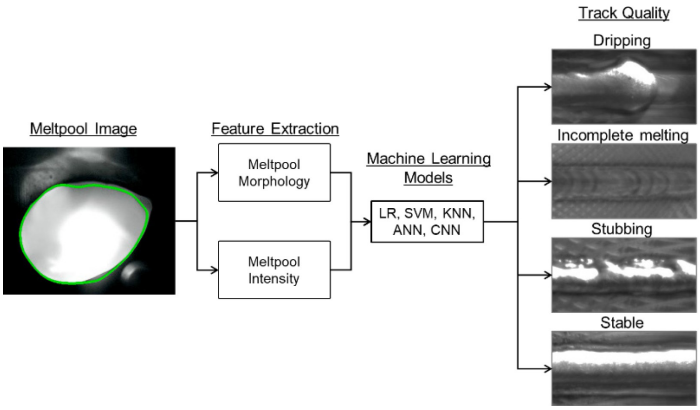

FIGURE 6: OVERVIEW OF PROCESS REGIME CLASSIFICATION USED IN THIS WORK.

Five algorithms with varying complexity were trained to detect the process regime. These models were: logistic regression (LR), support vector machine (SVM), k-nearest neighbors (KNN), artificial neural networks (ANN), and compared them to complex convolutional neural networks (CNN). These algorithms have been consistently used for manufacturing quality classification tasks in literature [5, 7, 8]. Further, we have directly used the meltpool images within a convolutional deep learning neural network (CNN).

All models used a 70/30 train-test split for training and testing where 70% of the data was used to train the algorithms (112, 410 images), while 30% of the data was used to test the algorithms (47, 462 images). All the images that originated from the same single-track were grouped together to avoid confounding variables. To tune the hyperparameters of the classification algorithms a 3-fold cross-validation approach was applied within the training dataset (37, 470 images per fold).

3. RESULTS AND DISCUSSION

3.1 Effect of Conditions on the Processing Regime

The effect of processing conditions on the processing regimes is depicted in FIGURE 7. In the low wire feed rate conditions, the primary track qualities observed are stable and dripping regimes. In the high feed rate conditions stubbing and incomplete melting can be observed due to the increase in linear mass density.

Under the low wire feed rate regime, as the laser power increases and scan speed decreases, the resultant energy density increases. As the energy density increases the wire begins melting prior to reaching the laser focal point on the meltpool. This results in a molten material that 'drips' globular material onto the single-track and generates large line width variation.

Then as the scan speed increases, the process drifts towards stable due to the decrease in the resultant energy density. This decrease in energy density ensures that the wire is melting at the focal point of the meltpool and depositing a healthy single-track. However, as the scan speed keeps increasing, not enough of the wire is melted fast enough, resulting in the stubbing of the wire into the substrate. Finally, this process drifts forwards incomplete melting under extreme increases in the scan speed relative to the laser power and wire feed rates. Under these conditions there is an extreme lack of energy density and the wire is never properly melted to generate the meltpool.

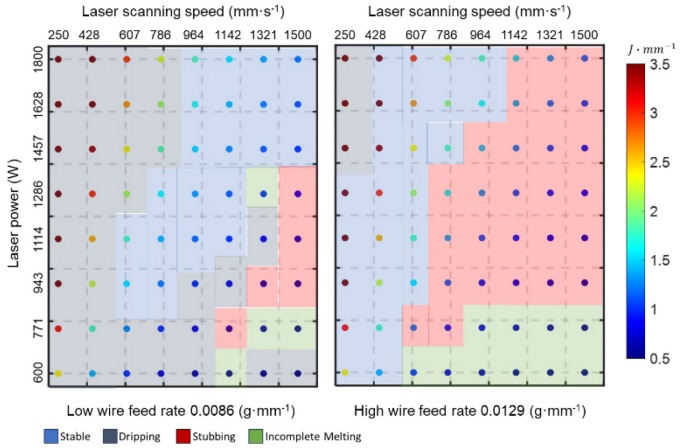

FIGURE 7: REGIME MAP FOR THE VARYING LASER POWERS AND SCAN SPEEDS USED IN THIS WORK.

Each of the four track quality conditions results in a variance in the meltpool penetration depth and single-track width. Under the stable condition, single-tracks have small levels of remelting into the substrate material as shown in FIGURE 8. As the process stability shifts toward dripping, the resultant meltpool depth increases due to the increased energy density penetrating deeper into the meltpool. Additionally, under the dripping regime, the meltpool width increases substantially where the dripping material interacts with the deposited single-track. As the process shifts towards stubbing, both the penetration depth and resultant single-track width decrease substantially. This is due to the lack of input energy density resulting in a condition very similar to the balling regime in LPBF. Finally in the incomplete melting regime, due to a complete breakdown of the meltpool there is no single-track to observe in FIGURE 8.

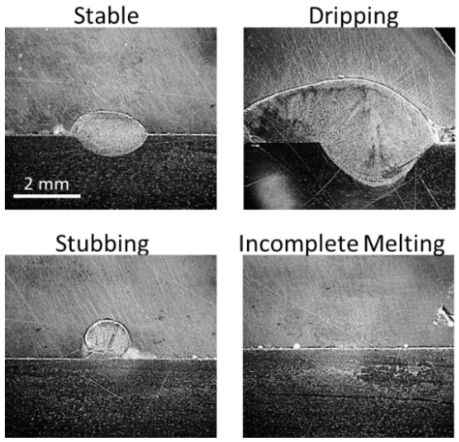

FIGURE 8: COMPARISON OF SINGLE-TRACK CROSS-SECTIONS FOR STABLE, DRIPPING, STUBBING AND INCOMPLETE MELTING REGIMES.

3.2 Effect of Conditions on the Meltpool

The resulting meltpool image from each treatment condition is visualized in FIGURE 9 where exemplar meltpool images from the high-speed imaging camera are depicted. Clear visual trends in the meltpool shape and brightness are seen as the processing parameters change. These changes in the meltpool are the source of the errors observed in the resultant single-tracks in this work. For brevity, we restrict our discussion herein to the meltpool morphology and intensity features.

For example, as the energy density increases, under both wire feed rates, the meltpool becomes bigger and brighter as more material is being melted. This large meltpool generates the dripping regime discussed in the previous section. Then as the energy decreases the meltpool continuously becomes smaller and dimmer resulting in the stubbing and incomplete melting regimes. Under the stable regime, highlighted in blue, the meltpool appears to be ovular with a bright center and a dim tail.

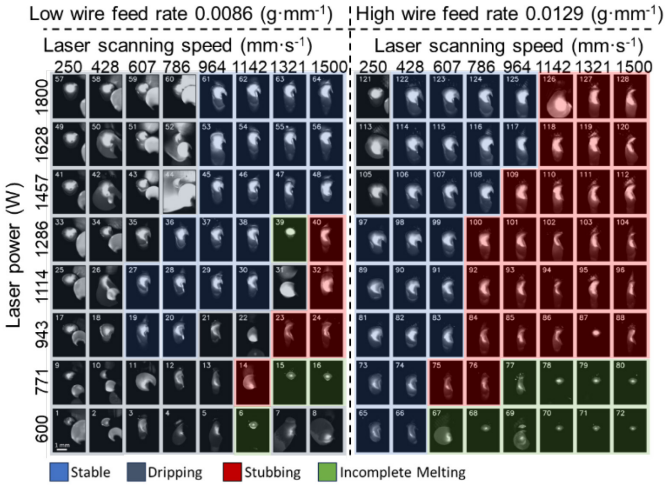

FIGURE 9: EXAMPLE MELTPOOL IMAGES FOR EACH SINGLE-TRACK BUILT UNDER VARYING PARAMETERS.

These visual changes in the meltpool images can be quantified and analyzed using the computer vision approach depicted in FIGURE 5. After identifying the meltpool boundary meltpool morphology and intensity features can be extracted to monitor the process stability.

Three meltpool morphology features were found to be necessary for process monitoring in this work. These three features were meltpool area, aspect ratio, and irregularity.

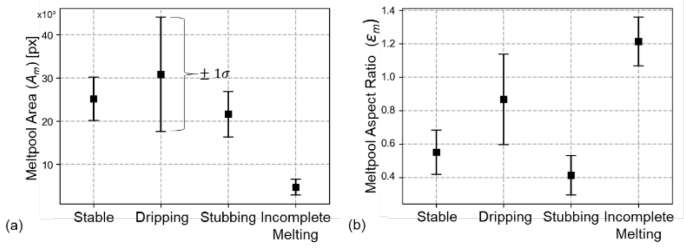

FIGURE 10: FEATURES` MEAN AND STANDARD DEVIATION ARE PLOTTED FOR EVERY PROCESS REGIME IN (A) FOR THE MELTPOOL AREA, (B) FOR THE MELTPOOL ASPECT RATIO.

The meltpool area (A_m), serves as a distinguishing factor both for the dripping and the incomplete melting regime. Incomplete meltpools are distinguishable by their relatively smaller meltpools. Dripping regime meltpools, on the other hand, exhibit the larges areas and are impacted by the greatest level of variability (FIGURE 10(a)).

The meltpool aspect ratio (ε_m), acts as a strong discriminator between the group of dripping and incomplete melting regimes, and the group of stable and stubbing. Both stubbing and stable regimes produce elliptical meltpools which can be observed in FIGURE 9. Dripping and incomplete melting generate circular meltpools despite being on opposite end of the energy density spectrum (FIGURE 10(b)).

Finally, the meltpool irregularity (σ_m), was found to be an important factor in the detection of regime qualification. Meltpool irregularity measures the deviation of the meltpool from a perfect circle based on around a centroid. This results in similar results as the aspect ratio of the meltpool. However, irregularity of the meltpool depicts differences between the stubbing and stable processing regime in which stubbing is found to be more irregular in shape than the stable conditions.

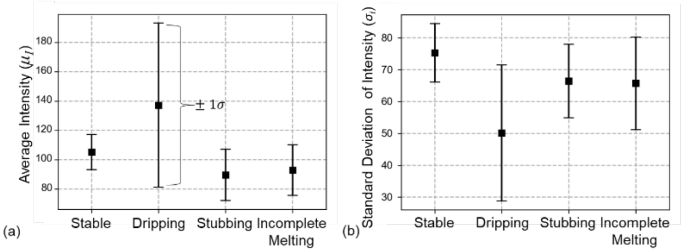

FIGURE 11: FEATURES MEAN AND STANDARD DEVIATION ARE PLOTTED FOR EVERY PROCESS REGIME FOR (A) AVERAGE & (B) STANDARD MELTPOOL BRIGHTNESS.

In addition to analyzing meltpool morphology features, meltpool intensity-based features were also extracted in the form of meltpool brightness (intensity), standard deviation of brightness, and skewness of meltpool intensity. Meltpool average brightness (μ_I), shows a clear deviation from the dripping regime and the other three regimes (FIGURE 11 (a)). This is because the dripping regime occurs under the highest energy density and has the hottest meltpools resulting in the brightest pixels. The large standard deviation is caused by some meltpool images being the dripping regime which creates extremely bright and large meltpools. The next brightest meltpool regime is the stable regime as this occurs under the second highest energy density parameter sets.

The standard deviation of each meltpools brightness (σ_I) is another monitored feature. Upon investigation of this intensity feature, in FIGURE 11 (b), the deviation of meltpool intensity increases from the dripping, incomplete melting, stubbing, and stable regimes. This indicates that a healthy stable meltpool must have a large variation of temperatures inside of the meltpool. Likewise, the skewness of meltpool intensity (σ^3_I) was found to respond to the various regimes.

3.3 Process Regime Classification

Using the eight features discussed in the previous section, six supervised machine learning models of increasing complexity were trained on the 47,000 meltpool images as described in Sec. 2.3. The models used in this work were logistic regression, KNN, SVM, MLP, and CNN. The resultant testing F-scores for each model are visualized in TABLE 3 in which SVM performed the four-way classification the best with an F-score of 90.46%.

The SVM testing classification confusion matrix is shown in TABLE 4, which provides further insights of model performance. The columns represent the model's prediction and the rows represent the actual (manual) classification of the regime. Correct model predictions fall along the bolded diagonal and any numbers off the main axis are false predictions. Upon investigating the confusion matrix, it can be observed that there was minimal to no confusion between incomplete melting and the other three regimes. However, there are some misclassifications between the dripping regime and both the stable and stubbing regimes. This is to be expected as the standard deviation on each feature extracted for the dripping regime encompassed all the other regimes. Additionally, the only confusion for incomplete melting occurred between incomplete melting and the dripping regime. However, these misclassifications were not large enough to lower the F-score to 90%. The primary confusion in the model is between the stubbing and the stable regimes and is the primary reason for the model not performing better. This is also expected, as for all eight features extracted the stubbing and stable regimes either had similar or overlapping distributions. Future works will address this confusion by studying other morphological and intensity-based features and their ability to separate these two conditions. Additionally, various bandpass filters can be tested to identify which wavelengths of light provide the highest separation of intensity-based features.

TABLE 3: CLASSIFICATION PERFORMANCE FOR ALL TESTED MACHINE LEARNING ALGORITHMS

	Simple Data Fitting		Active Learning		Black-Box	
Model	Logistic Regression	KNN	**SVM**	MLP	CNN	VGG16
F-Score	89.95	85.67	**90.46**	88.16	87.35	87.53

TABLE 4: THE CONFUSION MATRIX FOR PROCESS REGIME CLASSIFICATION FROM THE SVM MODEL (F-SCORE > 90%).

		Predicted Regime			
		Dripping regime	Incomplete melting	Stubbing regime	Stable regime
Actual Regime	Dripping regime	**11513**	15	314	648
	Incomplete melting	14	**4982**	0	0
	Stubbing regime	533	0	**8153**	1306
	Stable regime	321	0	1906	**17757**

4. CONCLUSION

In this work, the process stability of the LW-DED process was successfully monitored and classified using a high-speed imaging camera with a fidelity of 90% F-score. The developed approach was able to classify the single-track quality into one of four regimes: stable, stubbing, incomplete melting, or dripping. This work extracts simple physics-based morphological and intensity features from the meltpool images. Doing so allows for a physical interpretability of the model, which is vital for implementation in industrial systems. High-speed imaging cameras generate terabytes of data per manufactured part if implemented in-situ. By extracting physics-based features, every large 2D image can be replaced with a small 1D vector of the eight features. Thus, enabling the deletion of the image while still storing meltpool information to review at a later date. This is a distinct advantage to data-based models, such as CNNs, in which the raw images need to be stored if the data needs to be reviewed post-build.

Future works will first test the model transferability between machine-to-machine and material-to-material. This is an important step to ensure model robustness and quality predictions across various machine platforms. Then future works will build upon this model and attempt to monitor the quality of functional, complex 3D parts manufactured using LW-DED. This is a prerequisite step for in-situ part qualification of the LW-DED processes which is the long-term objective of this work. Additionally, future works will aim to use high-speed imaging data to predict the evolved microstructure found in manufactured samples.

ACKNOWLEDGEMENTS

This work was supported by the National Science Foundation (NSF) for funding his work under awards CMMI-2309483/1752069,OIA-1929172,PFI-TT 2322322/2044710, CMMI-1920245, ECCS-2020246, CMMI-1739696, and CMMI-1719388.

REFERENCES

[1] T.E. Abioye, J. Folkes, A.T. Clare, A parametric study of Inconel 625 wire laser deposition, Journal of Materials Processing Technology 213(12) (2013) 2145-2151. https://doi.org/10.1016/j.jmatprotec.2013.06.007

[2] M. Motta, A.G. Demir, B. Previtali, High-speed imaging and process characterization of coaxial laser metal wire deposition, Additive Manufacturing 22 (2018) 497-507. https://doi.org/10.1016/j.addma.2018.05.043

[3] B.T. Gibson, Y.K. Bandari, B.S. Richardson, W.C. Henry, E.J. Vetland, T.W. Sundermann, L.J. Love, Melt pool size control through multiple closed-loop modalities in laser-wire directed energy deposition of Ti-6Al-4V, Additive Manufacturing 32 (2020) 100993. https://doi.org/10.1016/j.addma.2019.100993

[4] L. Chen, X. Yao, Y. Chew, F. Weng, S.K. Moon, G. Bi, Data-Driven Adaptive Control for Laser-Based Additive Manufacturing with Automatic Controller Tuning, Applied Sciences, 2020. 10.3390/app10227967

[5] N.D. Jamnikar, S. Liu, C. Brice, X. Zhang, In-process comprehensive prediction of bead geometry for laser wire-feed DED system using molten pool sensing data and multi-modality CNN, The International Journal of Advanced Manufacturing Technology 121(1) (2022) 903-917. 10.1007/s00170-022-09248-3

[6] X. Xu, G. Mi, Y. Luo, P. Jiang, X. Shao, C. Wang, Morphologies, microstructures, and mechanical properties of samples produced using laser metal deposition with 316L stainless steel wire, Optics and Lasers in Engineering 94 (2017) 1-11. https://doi.org/10.1016/j.optlaseng.2017.02.008

[7] A. Gaikwad, R.J. Williams, H. de Winton, B.D. Bevans, Z. Smoqi, P. Rao, P.A. Hooper, Multi phenomena melt pool sensor data fusion for enhanced process monitoring of laser powder bed fusion additive manufacturing, Materials & Design 221 (2022) 110919. https://doi.org/10.1016/j.matdes.2022.110919

[8] Z. Smoqi, A. Gaikwad, B. Bevans, M.H. Kobir, J. Craig, A. Abul-Haj, A. Peralta, P. Rao, Monitoring and prediction of porosity in laser powder bed fusion using physics-informed meltpool signatures and machine learning, Journal of Materials Processing Technology 304 (2022) 117550. https://doi.org/10.1016/j.jmatprotec.2022.117550